Kv4 potassium channel subunits control action potential repolarization and frequency-dependent broadening in rat hippocampal CA1 pyramidal neurones

Jinhyun Kim, Dong-Sheng Wei and Dax A. Hoffman

Molecular Neurophysiology and Biophysics Unit, Laboratory of Cellular and Synaptic Neurophysiology, National Institute of Child Health and Human Development, National Institutes of Health, Bethesda, MD 20892, USA

A-type potassium channels regulate neuronal firing frequency and the back-propagation of action potentials (APs) into dendrites of hippocampal CA1 pyramidal neurones. Recent molecular cloning studies have found several families of voltage-gated K^+ channel genes expressed in the mammalian brain. At present, information regarding the relationship between the protein products of these genes and the various neuronal functions performed by voltage-gated K^+ channels is lacking. Here we used a combination of molecular, electrophysiological and imaging techniques to show that one such gene, Kv4.2, controls AP half-width, frequency-dependent AP broadening and dendritic action potential propagation. Using a modified Sindbis virus, we expressed either the enhanced green fluorescence protein (EGFP)-tagged Kv4.2 or an EGFP-tagged dominant negative mutant of Kv4.2 ($Kv4.2g^{W362F}$) in CA1 pyramidal neurones of organotypic slice cultures. Neurones expressing $Kv4.2g^{W362F}$ displayed broader action potentials with an increase in frequency-dependent AP broadening during a train compared with control neurones. In addition, Ca^{2+} imaging of $Kv4.2g^{W362F}$ expressing dendrites revealed enhanced AP back-propagation compared to control neurones. Conversely, neurones expressing an increased A-type current through overexpression of Kv4.2 displayed narrower APs with less frequency dependent broadening and decreased dendritic propagation. These results point to Kv4.2 as the major contributor to the A-current in hippocampal CA1 neurones and suggest a prominent role for Kv4.2 in regulating AP shape and dendritic signalling. As Ca^{2+} influx occurs primarily during AP repolarization, Kv4.2 activity can regulate cellular processes involving Ca^{2+}-dependent second messenger cascades such as gene expression and synaptic plasticity.

(Resubmitted 20 July 2005; accepted after revision 30 August 2005; first published online 1 September 2005)
Corresponding author D. Hoffman: Molecular Neurophysiology and Biophysics Unit, Laboratory of Synaptic and Cellular Neurophysiology, National Institute of Child Health and Human Development, National Institutes of Health, Porter Neuroscience Research Center, 35 Lincoln Drive, Building 35, Room 3C-905, Bethesda, MD 20892-3715, USA. Email: hoffmand@mail.nih.gov

The fine-tuning of neuronal electrical signals is achieved predominantly by the action of voltage-gated K^+ channels. Over 35 different primary K^+ channel subunits are expressed in the hippocampus (Coetzee *et al.* 1999). This diverse set of K^+ channel subtypes allows for the distinctive firing patterns expressed by different neurone types and by the same cells under different conditions.

The total outward K^+ current recorded in hippocampal CA1 pyramidal neurones consists of a transient or rapidly inactivating component (A-type) and a sustained or slow/non-inactivating component (Rudy, 1988; Storm, 1990). Of the numerous known voltage-gated K^+ channel (Kv) pore-forming α-subunits expressed in the hippocampus, only Kv1.4, Kv4.1, Kv4.2 and Kv4.3 produce subthreshold activating, fast inactivating, 4-aminopyridine (4-AP)-sensitive currents that resemble the A-type current in CA1 neurones (Coetzee *et al.* 1999). Immunohistochemical data show that Kv4.2 is the most likely molecular counterpart to the A-current recorded in hippocampal CA1 dendrites, with high expression in the somatodendritic membrane (Sheng *et al.* 1992; Maletic-Savatic *et al.* 1995; Serodio *et al.* 1996; Varga *et al.* 2000). Kv1.4 is primarily found in axons, Kv4.1 is not highly expressed in the hippocampus and hippocampal Kv4.3 is primarily found in interneurones (Serodio & Rudy, 1998; Coetzee *et al.* 1999; Lien *et al.* 2002; Rhodes *et al.* 2004).

Previous studies have used various molecular techniques to link voltage-clamp analyses of A-type

 DOI: 10.1113/jphysiol.2005.095042

currents with particular Kv α-subunits. Using single-cell RT-PCR, Kv4 family mRNAs have been observed in several different neuronal types (Baro *et al.* 1997; Martina *et al.* 1998; Song *et al.* 1998; Tkatch *et al.* 2000). Other groups have used dominant negative Kv4 constructs to show that α-subunits of the Kv4 subfamily underlie the transient current in cerebellar granule neurones (Johns *et al.* 1997; Shibata *et al.* 2000) and superior cervical ganglion neurones (Malin & Nerbonne, 2000).

A-type currents in CA1 hippocampal neurones have important roles in dendritic signal processing, including the regulation of AP back-propagation, synaptic integration (Hoffman *et al.* 1997; Cash & Yuste, 1998; Ramakers & Storm, 2002; Cai *et al.* 2004), and in long-term potentiation (Ramakers & Storm, 2002; Watanabe *et al.* 2002; Frick *et al.* 2004). Modulation of A-type current's biophysical properties and expression levels occurs through phosphorylation or auxiliary subunits (Hoffman & Johnston, 1998; An *et al.* 2000; Anderson *et al.* 2000; Beck *et al.* 2002; Yuan *et al.* 2002; Nadal *et al.* 2003; Gebauer *et al.* 2004; Varga *et al.* 2004). This high degree of regulation suggests a central role for A-channels in modulating neuronal excitability.

The experiments presented here were undertaken to test directly the hypothesis that Kv4.2 underlies the A-current in CA1 hippocampal pyramidal neurone somatodendritic membrane and to investigate its role in shaping CA1 firing patterns. We used a modified Sindbis virus system to either overexpress wild-type Kv4.2 or a dominant negative mutant of Kv4.2 (Kv4.2g^{W362F}) in hippocampal organotypic slice cultures. Tagged Kv4.2 was found to mimic the endogenous Kv4.2 somatodendritic expression pattern with the interesting discovery of enriched expression in dendritic spines. Kv4.2g^{W362F} expression led to broader APs with an increase in frequency-dependent AP broadening and enhanced dendritic propagation. Conversely, Kv4.2 overexpression dampened cell excitability most notably by decreasing AP half-width, frequency-dependent AP broadening and dendritic AP propagation.

Methods

Hippocampal cultures and viral infection

Hippocampal primary cultures were prepared from embryonic day 18 Sprague-Dawley rats after pregnant mothers were killed by decapitation under isoflurane anaesthesia. Cells were cultivated in neurobasal medium supplemented with B27 (Invitrogen) as described by Osten *et al.* (1998). To eliminate proliferative cells, 5 μM cytosine arabinoside (AraC, Sigma), a specific inhibitor of DNA synthesis during meiosis and mitosis, was included on 8 days *in vitro* (DIV). Mature primary neurones (18 DIV−21 DIV) were infected with a normalized infectious titre of Sindbis virus (see Supplemental Material).

Hippocampal organotypic slice cultures were prepared from postnatal day 7–8 Sprague-Dawley rats, killed via cervical decapitation, after Musleh *et al.* (1997). Hippocampal slices (250 μm thick) were infected on 4 DIV by microinjection. Electrophysiological and Ca^{2+} imaging measurements were made 1–3 days after CA1 viral infection. All animal protocols were approved by the National Institute of Child Health and Human Development's Animal Care and Use Committee.

Immunostaining and image analysis

Infected dissociated neurones were fixed with 4% paraformaldehyde and 0.1% glutaraldehyde in PBS containing 0.12 M sucrose for 8 min and permeabilized with 0.2% Triton X-100 in PBS. After preblocking with PBS containing 5% normal goat serum (NGS), 0.05% Triton X-100, and 450 mM NaCl for 1 h at 4°C, neurones were incubated with antibodies in the blocking solution overnight at 4°C and followed by incubation with Alexa 546-conjugated secondary antibodies (Molecular Probes) at 1 : 200 dilution for 2 h at room temperature. Images were acquired with Leica TCS RS confocal microscope. Linear Profile Plot and ROI manager of ImageJ v. 1.32 (http://rsb.info.nih.gov/ij/) were used for spine expression analysis. The same mask of ROI (region of interest) was utilized for selection of dendritic spine heads and adjacent dendritic shafts. Antibodies used were anti-MAP2 (Chemicon, 1 : 1000) and anti-Synaptophysin (Sigma, 1 : 200)

Electrophysiology

For patch-clamp recordings, organotypic slice cultures or cover slips containing HEK-293 cells were transferred to a submerged recording chamber with continuous flow of ACSF containing (mM): 125 NaCl, 25 $NaHCO_3$, 2.5 KCl, 1.25 NaH_2PO_4, 2 $CaCl_2$, 1 $MgCl_2$, and 25 D-glucose bubbled with 5% CO_2−95% O_2. In some experiments 3–5 mM 4-AP was included in the bath solution. In these instances 0.01 mM 6,7-dinitroquinoxaline 2,3(1H,4H)-dione (DNQX) was also included in the external solution. DNQX was dissolved in DMSO (final DMSO concentration: 0.1%).

Hippocampal CA1 pyramidal neurones or HEK-293 cells were identified using infrared differential interference contrast (IR-DIC) videomicroscopy. The patch electrodes (2–5 MΩ) were filled with (mM): 125 potassium gluconate, 20 KCl, 10 Hepes, 4 NaCl, 0.5 EGTA, 10 disodium phosphocreatine, 4 ATP-Mg, 0.3 $Tris_2GTP$ (pH 7.2 with KOH). Recordings were low-pass filtered at 5 kHz and digitized at 10 kHz by an Instrutech ITC-18 A/D

board controlled by software written for Igor Pro (WaveMetrics).

Whole-cell CA1 recordings were made in current-clamp mode using either an Axopatch-200B or Multiclamp 700B amplifier (Axon Instruments) at 32–34°C. Series resistance was 10–28 MΩ. Typically, current injection series were repeated three times and the results reported as the average of the three individual measurements. Voltages have not been corrected for junction potentials.

Recordings of voltage-gated K^+ currents were made in voltage-clamp mode using the Axopatch-200B amplifier at room temperature. Electrodes were pulled from borosilicate glass and in some experiments coated with Sylgard (Dow Corning) to reduce their capacitance. Current ensemble averages were constructed from 3 to 30 individual sweeps. Leakage and capacitive currents were subtracted digitally using either a P/5 protocol or null traces. The transient current was isolated from the sustained current using a 150 ms prepulse step to −20 mV to inactivate transient channels. All curve fits (inactivation time constants, Boltzmann fits and various $x-y$ plots) were performed with a least-squares program (Igor Pro). In outside-out and nucleated patch recordings, 1 μM TTX (Sigma) was included in the bath. The capacitative compensation circuit of the amplifier was used to measure and reduce capacitative transients. Nucleated patches had an average capacitance of 1.53 ± 0.03 pF ($n = 18$) corresponding to a diameter of ∼7 μm (Martina *et al.* 1998). Outside-out patch capacitance was estimated to be 0.4 pF by comparing current amplitudes with those from nucleated patch recordings.

Calcium imaging

Patch pipettes (3–8 MΩ) were filled with (mM) 130 $KMeSO_4$, 10 Hepes, 4 $MgCl_2$, 4 Na_2-ATP, 0.4 Na_2-GTP, 10 Na_2-phosphorcreatine, and 3 sodium L-ascorbate. After obtaining whole-cell configuration, 20–30 min were allowed for intracellular diffusion of the fluorophore (Rhod-2, 100 μM, Molecular Probes). Optical data were acquired using a Roper Scientific MicroMax 512BFT CCD camera with 50 ms exposure time per frame. Action potentials were elicited by somatic current injection (1–2 nA, 2 ms). Trains of three action potentials were elicited at 100 Hz. Background fluorescence, estimated by averaging fluorescence of an equivalent position in the slice that contained no infected neurones, was subtracted for analysis.

Data analysis

Data analysis was performed using Igor Pro, SigmaStat, SPSS and Microsoft Excel. Numeric values are given as means ± standard error of the mean (S.E.M.). Error bars in the figures represent S.E.M. Statistical significance was examined with Student's *t* test, one-way ANOVA or Wilcoxon-Mann-Whitney test.

Results

Kv4.2 construct expression

To visualize Kv4.2, the enhanced green fluorescence protein (EGFP) was fused to either the cytoplasmic N- (gKv4.2) or C-terminal (Kv4.2g, Fig. S1*A* in Supplementary Material). When expressed in HEK-293 cells, EGFP-tagged Kv4.2 constructs and untagged Kv4.2 showed a single protein band of the expected size on a Western blot prepared from cell extracts (Fig. S1*B*). The same blot probed with a GFP antibody showed identical bands for both EGFP-tagged Kv4.2 constructs without any bands of unexpected size (data not shown). Both EGFP-tagged proteins displayed a distinct perinuclear, endoplasmic reticulum expression pattern in HEK-293 cells (Fig. S1*C*), as previously found in cells expressing untagged Kv4.2 (An *et al.* 2000; Nadal *et al.* 2003; Shibata *et al.* 2003).

An investigation into the normal physiological role of particular ion channels requires that the kinetic properties of heterogolously expressed channels closely match those of the native protein. To determine the effect of EGFP fusion on Kv4.2 we compared the properties of N- and C-terminal EGFP-fused Kv4.2 to those of untagged Kv4.2, after expression in HEK-293 cells. Currents recorded from both gKv4.2- and Kv4.2g-expressing cells had activation curves nearly identical to that found for untagged Kv4.2 ($P > 0.05$, Table 1). Similarly, no significant differences were found for the inactivation curves of either EGFP fused channel compared with Kv4.2 ($P > 0.05$, Table 1). While attachment of EGFP to the channel was not found to affect steady-state inactivation, the *rate* of inactivation was slowed by N-terminal but not C-terminal EGFP fusion (Table 1; Wong *et al.* 2002). Despite a slower inactivation rate, there was not a significant effect of EGFP fusion on the time course of recovery from inactivation ($P > 0.05$, Table 1). Given the results from these HEK-293 experiments, we chose to use Kv4.2g for further investigation in neurones.

To reduce functional Kv4.2-mediated conductance in neurones, a point mutation was introduced in the pore of Kv4.2 (W362 to F) which has been used previously to down-regulate Kv4.2 activity in superior cervical ganglion neurones (Malin & Nerbonne, 2000, 2001; Wong *et al.* 2002). The $Kv4.2g^{W362F}$ mutation has been shown previously to act as a subfamily-specific dominant negative, i.e. blocking only Kv4.x or *shal*-containing channels after heterologous expression (Barry *et al.* 1998). Co-expression in HEK-293 cells of equal amounts $Kv4.2g^{W362F}$ and Kv4.2 attenuated the wild-type currents

Table 1. Expression level, voltage dependence and kinetic properties of transient K^+ currents in HEK-293 cells and CA1 neurones of organotypic slice cultures

	Current density		Activation		Inactivation		Kinetics (room temp)		
	Transient (pA pF^{-1})	Sustained (pA pF^{-1})	$V_{1/2}$ (mV)	k	$V_{1/2}$ (mV)	k	t_{peak} (ms)	τ_{decay} (ms)	τ_{recov} (ms)
HEK-293 cell recordings									
Kv4.2	180 ± 55 (11)	—	−1.1 ± 1.5 (10)	17 ± 1 (10)	−71 ± 4 (10)	8.2 ± 0.9 (10)	6.0 ± 0.8 (9)	35 ± 4 (10)	96 ± 18 (8)
gKv4.2	209 ± 29 (14)	—	0.7 ± 1.1 (11)	18 ± 1 (11)	−69 ± 2 (10)	7.7 ± 0.3 (10)	6.3 ± 0.7 (5)	63 ± 6* (12)	94 ± 12 (9)
Kv4.2g	210 ± 52 (9)	—	0.9 ± 2.7 (9)	17 ± 2 (9)	−72 ± 3 (6)	7.1 ± 0.3 (6)	6.6 ± 0.6 (5)	37 ± 6 (8)	91 ± 14 (5)
Patch recordings from CA1 neurones of hippocampal slice cultures (DIV 5–7)									
Control	571 ± 66 (37)	79 ± 10 (37)	−15 ± 5 (14)	17 ± 1 (14)	−69 ± 3 (9)	8.7 ± 0.4 (9)	2.1 ± 0.4 (10)	26 ± 1 (34)	24 ± 4 (8)
Kv4.2g	1213 ± 157* (25)	100 ± 16 (25)	−13 ± 3 (10)	20 ± 2 (10)	−74 ± 3 (8)	9.2 ± 0.7 (8)	2.2 ± 0.1 (6)	19 ± 2* (22)	27 ± 4 (6)
Kv4.2g-W362F	345 ± 46* (22)	82 ± 13 (22)	−15 ± 3 (5)	20 ± 2 (5)	−75 ± 2 (7)	7.3 ± 0.9 (7)	2.1 ± 0.2 (5)	25 ± 4 (21)	28 ± 3 (6)

Values in parentheses, n number; $V_{1/2}$ and k, average fit half-activation and inactivation voltages and slope; t_{peak}, time to peak (+40 mV); τ_{decay}, single-exponential decay fit (+60 mV); τ_{recov}, single-exponential recovery fit (+60 mV); $^*P < 0.05$.

by 70% from 188 pA pF^{-1} ($n = 13$) to 57 pA pF^{-1} ($n = 14$, data not shown).

Expression of Kv4.2 constructs in neurones

To introduce Kv4.2g and Kv4.2g^{W362F} into neurones, we used an attenuated Sindbis virus-based expression system. This modified system has been shown, in hippocampal primary neurones and *in vivo*, to delay the onset of viral-induced cytotoxicity and produce higher expression levels of the protein of interest (Kim *et al.* 2004). In cultured hippocampal neurones Kv4.2g mimicked the somatodendritic expression pattern found for endogenous Kv4.2 (Fig. 1*A*, top). Higher magnification images show clearly that Kv4.2g is expressed in dendritic spines (Fig. 1*A*, bottom). Kv4.2-positive spines were found apposed to the presynaptic marker, synaptophysin (Fig. 1*B*). The EGFP fluorescence in spines of Kv4.2g expressing neurones appeared brighter than that from the adjacent dendritic shaft (Fig. 1*C*). To quantify this observation we compared the relative fluorescence intensity in spines with that of the adjacent dendritic shaft. The ratio of spine head to dendritic shaft fluorescence in Kv4.2g-expressing neurones was approximately 2-fold greater than in neurones expressing EGFP (1.90 ± 0.07, $n = 117$ spines from 10 dendrites for Kv4.2g *versus* 0.84 ± 0.02, $n = 105$ spines from 8 dendrites, EGFP, Fig. 1*C* and *D*). These results, showing postsynaptic expression and spine enrichment of Kv4.2g in hippocampal neurones, support a previous report on endogenous Kv4.2 localization that found Kv4.2 clustered at synaptic sites using immuno-electron microscopy (Alonso & Widmer, 1997).

We next expressed the mutant Kv4.2 constructs in CA1 pyramidal neurones of hippocampal slices (Fig. 2*A*). Three experimental groups were analysed: control neurones (either uninfected or EGFP expressing), neurones overexpressing Kv4.2 (Kv4.2g), and neurones expressing the dominant negative Kv4.2 pore mutation (Kv4.2g^{W362F}). Infected neurones were not visually different from neighbouring uninfected neurones and no significant changes in endogenous K^+ channel protein levels were observed in Kv4.2g-infected slices compared with uninfected or EGFP-infected control slices (Kv4.2, Kv1.4 and Kv2.1 compared by immunoblot, not shown). Whole-cell recordings revealed no significant difference in resting membrane potential (−60.3 ± 0.7 mV, Kv4.2g; −58.7 ± 0.7 mV, control and −58.6 ± 1.5 mV for Kv4.2g^{W362F}, $P > 0.05$) between groups.

Nucleated and outside-out patch-clamp recordings from CA1 hippocampal neurones, in the presence of TTX to block voltage-gated Na^+ channels, showed a large outward current composed of a rapidly inactivating component along with a sustained or slowly inactivating component (Fig. 2*A*). The transient current was isolated from the sustained current using a prepulse voltage protocol (see Methods). Patches pulled from neurones overexpressing Kv4.2 showed a 2-fold increase in transient outward current density compared with non-expressing control neurones, ($P < 0.05$) without affecting the sustained component density (Fig. 2*A* and *B*, Table 1, $P > 0.05$). Currents from both groups were similarly blocked by 3 mM 4-AP (control, 55 ± 7% block, $n = 9$; Kv4.2g, 58 ± 7% block, $n = 7$, data not shown). Expressing

the dominant negative Kv4 mutation knocked down the transient outward current density to 63% of control ($P < 0.05$), again without affecting the sustained outward current density (Fig. 2*A* and *B*, Table 1, $P > 0.05$). Transient current steady-state activation and inactivation were unaltered by Kv4.2g and Kv4.2g^{W362F} expression (Fig. 2*C* and *D*, Table 1, $P > 0.05$). Neither time-to-peak nor recovery from inactivation was affected in either experimental group (Table 1). As the W362F pore mutation functions as a dominant negative for all Kv4 channel homologues, these data do not themselves rule out a contribution of Kv4.1 or Kv4.3 channels to the A-current of the CA1 pyramidal neurone. However, paired with immunostaining and *in situ* data suggesting relatively

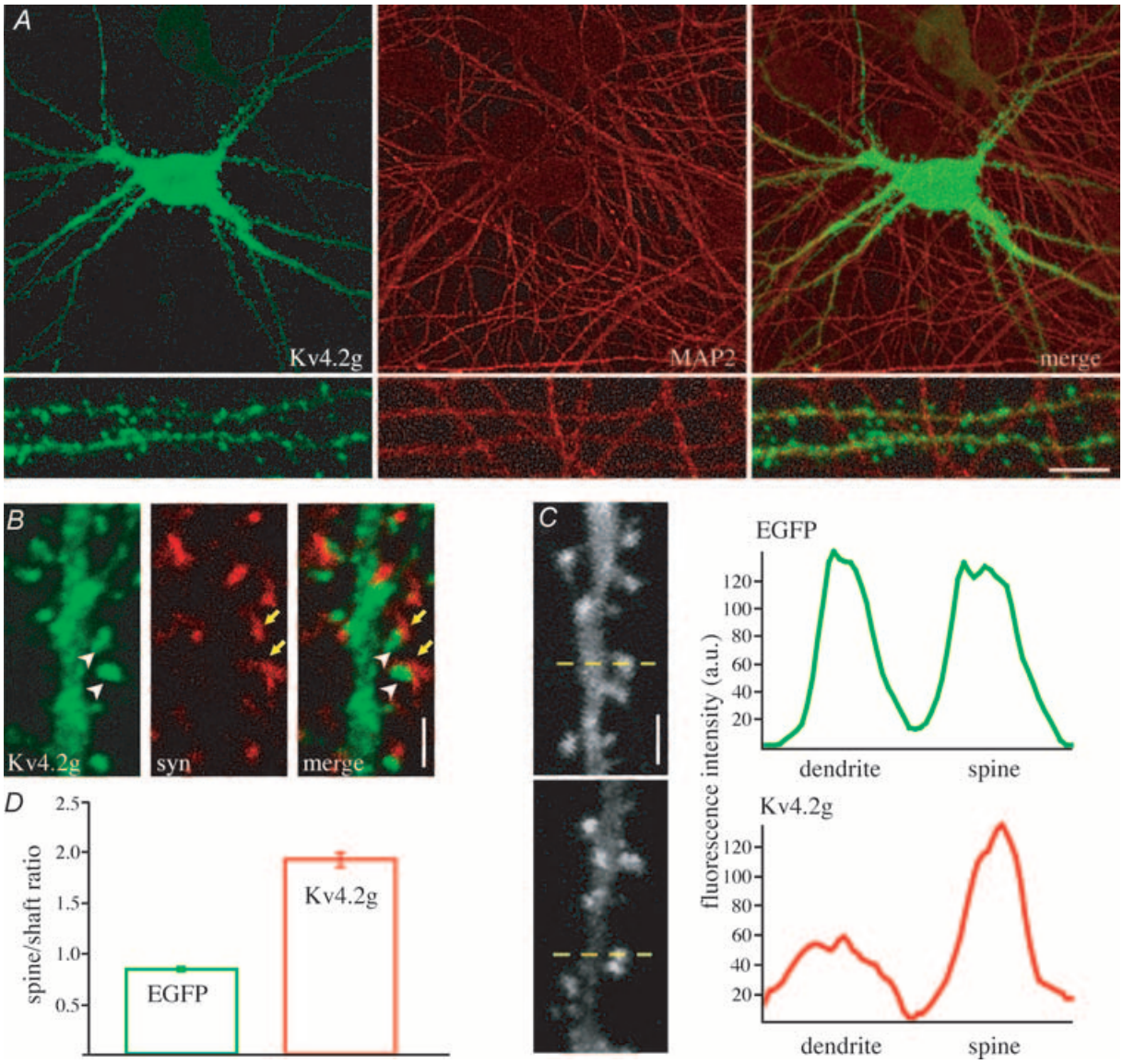

Figure 1. Somatodendritic expression and spine enrichment of Kv4.2g in cultured hippocampal neurones
A, attenuated Sindbis virus-mediated expression of Kv4.2g, detected by EGFP fluorescence, shows a somatodendritic distribution (left top) and is found in spines (left bottom). Most EGFP-positive spiny dendritic processes overlapped with MAP2-positive dendrites (right). No thin, axon-like processes were detected in Kv4.2g-expressing neurones. Scale bar: 8 μm. *B*, dual immunolabelling of Kv4.2g (white arrowhead) and the presynaptic marker synaptophysin (syn, yellow arrow), indicates postsynaptic expression of Kv4.2g. Scale bar: 4 μm. *C*, representative linear plot analysis of a dendritic shaft and spine. Comparison of the relative fluorescence intensity between dendritic shaft and spine showed that Kv4.2g was enriched in spines compared with EGFP alone. a.u., arbitrary units. Scale bar: 4 μm. *D*, summarized ratio of fluorescence intensity in spines relative to that in the adjacent dendritic shaft.

little Kv4.1 and Kv4.3 expression in CA1 pyramidal neurones (Serodio & Rudy, 1998; Rhodes *et al.* 2004) these data strongly implicate Kv4.2 as the main source of the somatodendritic A-current in CA1 neurones.

One difference in kinetics we did observe in CA1 neurones after Kv4.2g expression was a small but significant increase in the rate of inactivation of the transient current (Table 1). This result could indicate that Kv4.2g-expressing neurones have a different complement of modulatory auxiliary subunits. For example, overexpression of Kv4.2 channels may leave a pool of channels without a binding partner such as one of the KChIP (a small-molecular-weight calcium-binding protein) auxiliary proteins that have been shown to slow

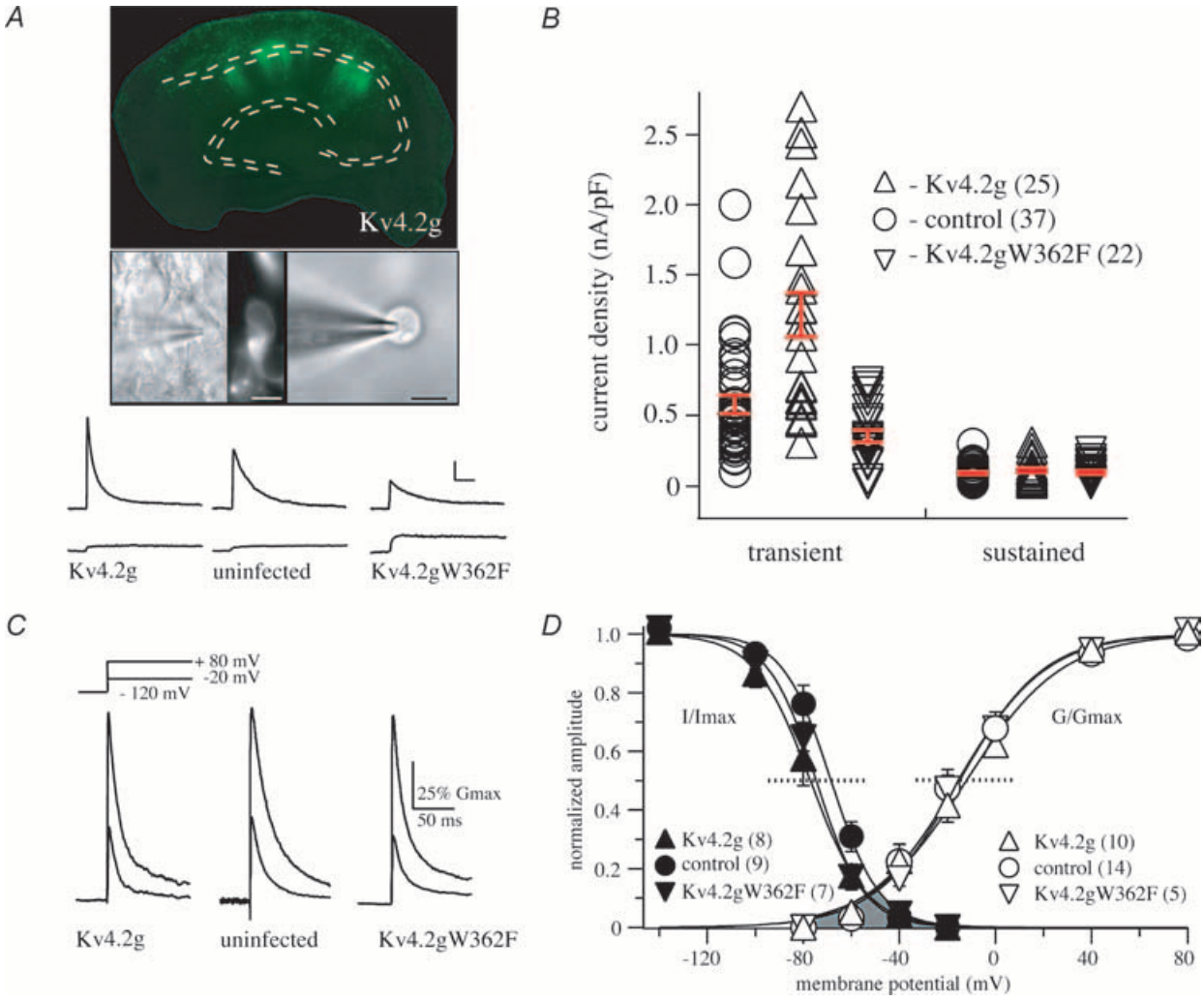

Figure 2. Nucleated and outside-out patch recordings from organotypic slice cultures
A, top, Kv4.2g fluorescence in CA1 neurones was imaged 1 day after infection; middle, high-powered IR-DIC image of a CA1 neurone with recording pipette; middle image shows the EGFP fluorescence of the same cell; right panel shows a nucleated patch. Scale bars: 10 μm. Bottom, representative voltage-isolated transient (top) and sustained outward currents (bottom) from Kv4.2g, uninfected and Kv4.2g^{W362F}-expressing neurones for voltage step from −120 to +60 mV. TTX (1 μM) was included in the bath to block Na^+ channels. Scale bar: 200 pA, 10 ms. *B*, transient and sustained peak current density per patch for Kv4.2g (△), Kv4.2g^{W362F} (▽), and control (uninfected or EGFP-expressing) neurones (○). *C*, isolated transient currents from nucleated patches from each experimental group for voltage steps from −120 to −20 and +80 mV. Each pair of traces was scaled to a normalized peak conductance. *D*, steady-state activation and inactivation curves for Kv4.2g, uninfected and Kv4.2g^{W362F} patches. Half-activation and inactivation voltages were not significantly different between groups. Numbers in parentheses indicate *n* values for inactivation and activation curves. Shaded grey area indicates the standing window current expected in uninfected cells.

down Kv4.2 inactivation rates, perhaps by favouring the slower pre-open closed inactivation state (An *et al.* 2000; Bahring *et al.* 2001; Jerng *et al.* 2004).

A comparison between Kv4.2g properties when expressed in HEK-293 cells *versus* in CA1 neurones suggests that another class of Kv4.2 auxiliary subunit binds to and modulates Kv4.2g channel properties in neurones. In CA1 neurones, all measured kinetics (time to peak, inactivation rate and rate of recovery from inactivation) are accelerated compared with those recorded in HEK-293 cells (Table 1). These differences can be attributed to a Kv4.2 auxiliary subunit (DPPX) expressed in CA1 neurones that has been shown to reconstitute the fast kinetics of native CA1 transient currents when expressed with Kv4.2 in a heterologous expression system (Nadal *et al.* 2003).

Kv4.2 and membrane excitability

To assess the contribution of Kv4 family subunits to membrane excitability and firing patterns of CA1 pyramidal neurones, whole-cell, current-clamp experiments were carried out in each of the three experimental groups. A series of 900 ms long current steps from −200 to +350 pA in 50 pA increments were delivered to cells in each group (Fig. 3*A*).

For subthreshold current injections from −60 mV, increasing the level of Kv4.2 expression (Kv4.2g) led to a substantial decrease in both peak and steady-state voltage deflections (Fig. 3*A*). Peak voltage reached for a hyperpolarizing 200 pA current injection was reduced from -90 ± 1 mV in control neurones ($n = 48$) to -81 ± 1 mV ($n = 28$, $P < 0.01$; Fig. 3*B*) in Kv4.2g neurones. The steady-state voltage reached was also reduced (-74 ± 1 mV, Kv4.2g *versus* -81 ± 1 mV for control; $P < 0.01$; Fig. 3*C* bottom trace). Conversely, decreasing functional Kv4.2 levels led to an increase in both peak and steady-state voltage deflections (Fig. 3*B*,*C*, $n = 15$, $P < 0.01$). Note in Fig. 3*A* (arrow) that the resulting steady-state voltage is not changed for a given initial peak voltage. Figure 3*D* shows that the voltage dependence of this 'sag' between peak and sustained voltage is preserved between experimental groups. The resistance at peak voltage (slope of the $I-V$ curve for the peak voltage) was dependent on resting potential and is increased with 4-AP (3–5 mM), both consistent with a role for Kv4.2 channels (Fig. 3*E*). These results show that Kv4.2 is open at rest in CA1 neurones, consistent with the window current found when plotting the transient current's steady-state activation and inactivation curves (grey area in Fig. 2*D*). This window current acts as a voltage shunt early during the current injection that determines the subsequent activation of currents such as I_h.

Figure 4*A* shows typical responses from Kv4.2g^{W362F}, control and Kv4.2g-expressing neurones in response to a suprathreshold 300 pA current injection. Recordings from Kv4.2g-expressing neurones displayed a delayed onset to first spike (Fig. 4*A* and *B*), which was followed by a distinctive large after-hyperpolarization potential (AHP, Fig. 4*A* and *C*). The average time until first spike increased from 33 ± 8 ms in controls ($n = 42$) to 87 ± 16 ms in Kv4.2g neurones ($n = 25$, $P < 0.01$, Fig. 4*B*). Onset time in Kv4.2g^{W362F}-expressing neurones was decreased compared with control (16 ± 8 ms, $n = 17$) although this change did not reach the level of significance. An increase in first spike latency was previously observed in CA1 neurones when transient current levels are increased by α-CaMKII phosphorylation of Kv4.2 (Varga *et al.* 2004).

The first spike AHP in Kv4.2g neurones (18 ± 1 mV, $n = 32$), measured as the voltage difference between AP threshold (Fig. 4*C*, filled arrow) and the peak after-hyperpolarization voltage (open arrow), more than doubled compared with control (8 ± 1 mV, $n = 45$, $P < 0.01$, Fig. 4*C*). No effect on first spike AHP amplitude was found for neurones expressing the dominant negative mutation (10 ± 1 mV, $n = 18$, $P > 0.05$, data not shown). AP firing threshold, measured in current ramps, was also significantly affected by Kv4.2g expression (-33 ± 1 mV, $n = 12$ *versus* -38 ± 2 mV, $n = 15$ for control, $P < 0.05$; Kv4.2g^{W362F}, -40 ± 2 mV, $n = 4$, $P > 0.05$). 4-AP (3–5 mM) was effective in countering the Kv4.2g effects on onset, AHP size and AP threshold (Fig. 4*B*–*D*).

The large AHP found in Kv4.2g-expressing neurones shows that Kv4.2 is strongly activated during AP depolarization, acting to repolarize the neurone. As such Kv4.2 would be expected to affect AP half-width. Accordingly, we found the AP half-width reduced in Kv4.2g-expressing cells (Fig. 5*A*, bottom traces) compared with control (Fig. 5*A*, middle traces) throughout a 300 pA current injection (Fig. 5*B*). APs recorded in Kv4.2g^{W362F}-expressing neurones were broader than control throughout the first half of the 900 ms current injection (Fig. 5*A*, top traces, Fig. 5*B*). Depolarizing the neurones to −50 mV, inactivating Kv4 channels, increased AP half-width while hyperpolarization, increasing the fraction of channels available for activation, reduced AP half-width (Fig. 5*B*). 4-AP (3–5 mM) significantly increased AP half-width for all three groups (4.4 ± 0.4 ms, Kv4.2g^{W362F}; 4.4 ± 0.5 ms, control; 2.6 ± 0.7 ms, Kv4.2g; APs binned over first 50 ms of the current injection, $P < 0.01$, data not shown).

Firing frequency was significantly reduced at the end of the current step with Kv4.2g overexpression and slightly increased in Kv4.2g^{W362F} neurones (Figs 4*A* and 5*C*). However, firing frequency over the first 100 ms of the current step was not significantly different between groups (Fig. 5*C* and *D*). Perhaps counter-intuitively, blocking Kv4 channels with 4-AP had no effect on frequency in any of the experimental groups (Fig. 5*D*).

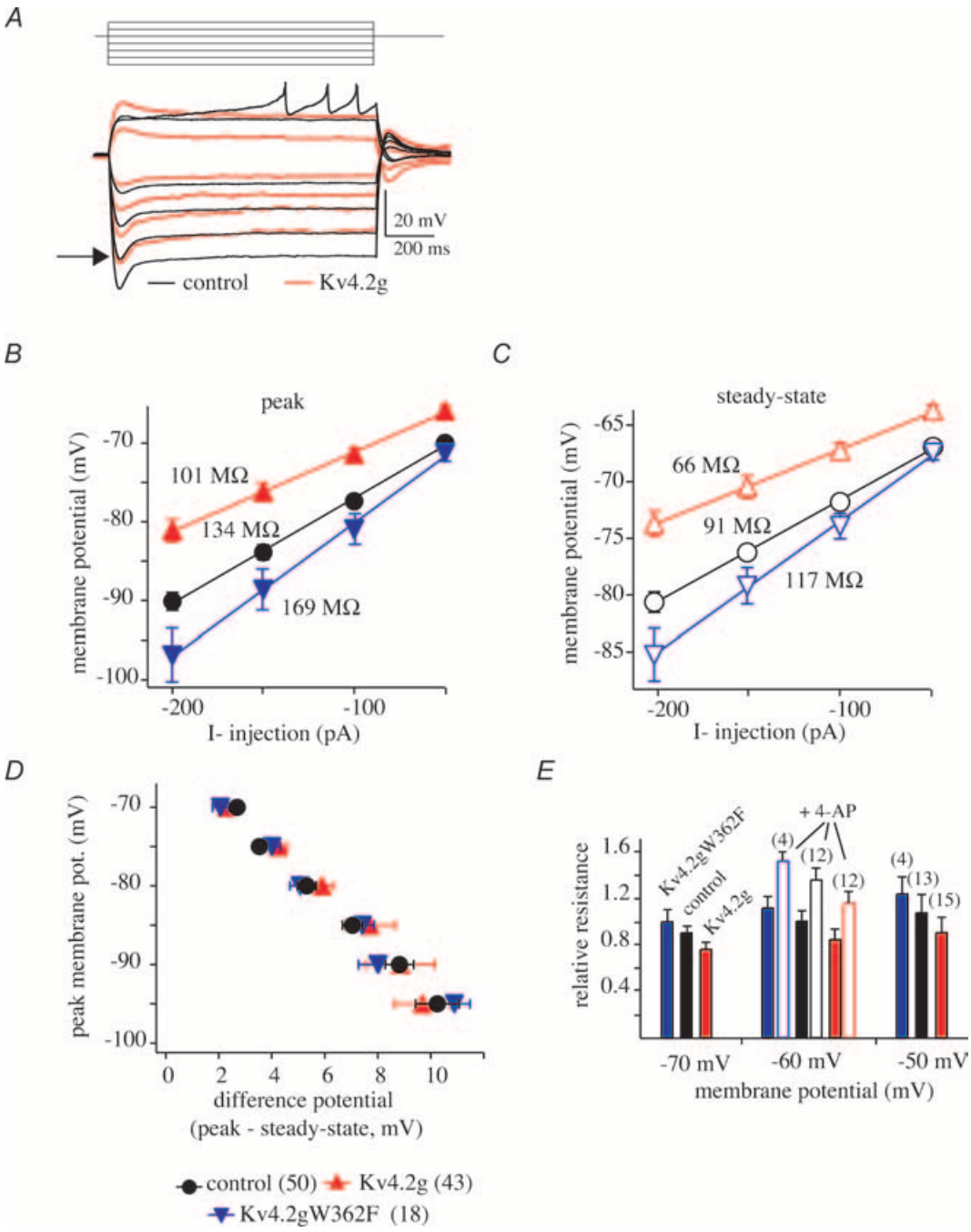

Figure 3. Kv4.2 activity affects cellular input resistance
A, subthreshold voltage transients generated in response to 900 ms current injections for Kv4.2g (red traces) and control neurones (black traces). Current injections were −200, −150, −100, −50, +50 and +100 pA. Smaller voltage responses are seen in the Kv4.2g cell for all injections. APs were initiated in the control cell in response to the +100 pA current injection (trace clipped for presentation) but not in Kv4.2-expressing cells. *B* and *C*, Current–voltage relationship for the peak (*B*) and steady-state (*C*) voltages for control cells (black circles), Kv4.2g- (red, up triangles), and Kv4.2g^{W362F}-expressing cells (blue, down triangles). Lines are linear regressions of the data. Overexpressing Kv4.2 lowered R_{in} while decreasing Kv4.2 levels increased R_{in}. *D*, the difference potential or 'sag' between peak and steady-state voltages is plotted against the peak voltage. This relationship did not differ between experimental groups. Same symbols as in *B*. *E*, resistance (slope of the *I*−*V* curve using the peak voltage) normalized to control at −60 mV, was dependent on resting potential ($P < 0.05$) in all groups and was increased with 4-AP (3–5 mM, $P < 0.05$).

These results can be explained by opposing influences of Kv4-mediated currents on firing frequency. Although current through Kv4 channels decreases frequency by countering subthreshold depolarization, they also narrow APs once initiated, thus creating the potential for increased frequency. These mixed influences explain why, although firing frequency was found to be voltage dependent ($P < 0.05$), we found no differences in frequency between experimental groups when current injections were initiated from the same membrane potential (Fig. 5*D*, $P > 0.05$). Taken together these data support a central role for Kv4-containing channels in regulating AP shape in CA1 pyramidal neurones. Below AP threshold, they counteract depolarization to delay AP onset and control firing frequency.

Frequency-dependent AP broadening

For all three groups, AP half-width increases during the AP train relative to the initial APs. That Kv4.2 inactivates rapidly but recovers from inactivation relatively slowly suggests a mechanism whereby cumulative Kv4.2 inactivation could mediate the observed AP broadening during a train. Such frequency-dependent AP broadening has been found in many cell types and in all neuronal compartments (Aldrich *et al.* 1979; Andreasen & Lambert, 1995; Ma & Koester, 1996; Shao *et al.* 1999; Geiger & Jonas, 2000; Faber & Sah, 2003).

To investigate the potential role of Kv4.2 in frequency-dependent AP broadening, 10 brief (5 ms), 800 pA current pulses were delivered at fixed frequencies

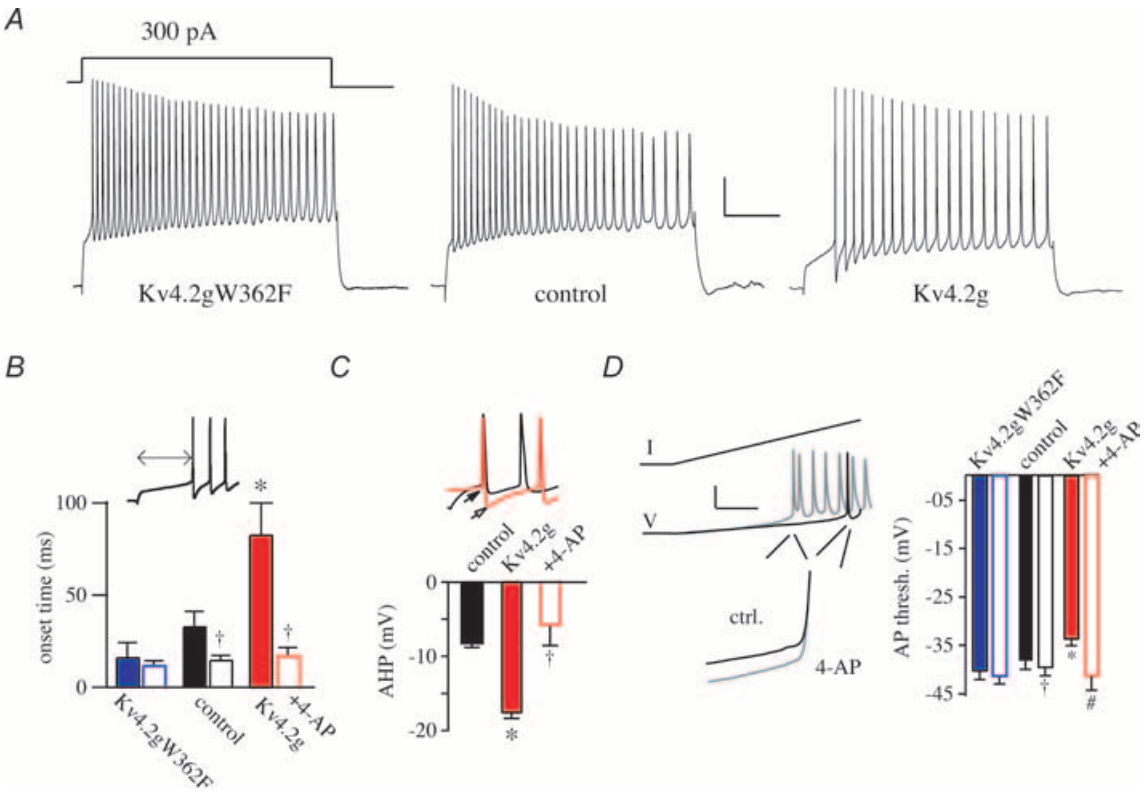

Figure 4. Kv4.2 overexpression increases AP latency, AHP and threshold
A, the voltage responses to a 900 ms, 300 pA current injection in Kv4.2g (right traces), control (middle traces), and Kv4.2g^{W362F} (left) neurones. Scale bar: 20 mV, 200 ms. *B*, time to first spike onset for control (black bar), Kv4.2g- (red bar), and Kv4.2g^{W362F} (blue bar) -expressing neurones for a 300 pA current injection. Open bars show that 4-AP reduced latency. *C*, enlarged traces from *A* (control, black trace; Kv4.2g, red trace), with the first APs aligned. The first spike AHP was measured as the voltage difference between AP threshold (filled arrow) and the peak after-hyperpolarization voltage (open arrow). Below, grouped data for the first AP AHP in control (black bar), Kv4.2g- (red bar), and Kv4.2g-expressing neurones in 3–5 mM 4-AP (open bar). $*P < 0.01$ *versus* control; †$P < 0.01$ *versus* Kv4.2g. *D*, top trace, representation of the current ramp (250 pA s^{-1}) used to determine AP threshold. Middle traces, the resulting voltages for a control neurone with normal (black trace) and 4-AP (grey trace) solutions. Scale bar: 20 mV, 100 ms. Bottom traces, same voltage traces as above aligned and magnified to illustrate threshold. Right, grouped AP threshold data. $*P < 0.01$ *versus* control; †$P < 0.05$ *versus* control; #$P < 0.01$ *versus* Kv4.2g.

of 10, 20, 50 and 100 Hz to neurones from each group (Fig. 6*A*). At frequencies greater than 10 Hz, AP half-width progressively increased during the train for all groups (Fig. 6*A*, left traces). To quantify broadening, we normalized AP half-width to that measured for the first AP of the train (Fig. 6*A*, right column). In control CA1 neurones, the second AP broadened to 148 ± 4% of the first at 100 Hz ($n = 18$), 129 ± 3% at 50 Hz, 108 ± 1% at 20 Hz but only 103 ± 1% at 10 Hz, demonstrating the frequency dependency of AP broadening in these cells (Fig. 6*A* and *B*, circles).

AP half-width was considerably reduced in Kv4.2g-expressing neurones. All 10 APs, at each frequency, displayed significantly reduced half-widths compared with control (Fig. 6*A*, left column, △, $n = 8$, $P < 0.01$). At higher stimulation frequencies (50 and 100 Hz), significantly less broadening occurred in Kv4.2g-expressing neurones than control for the first two

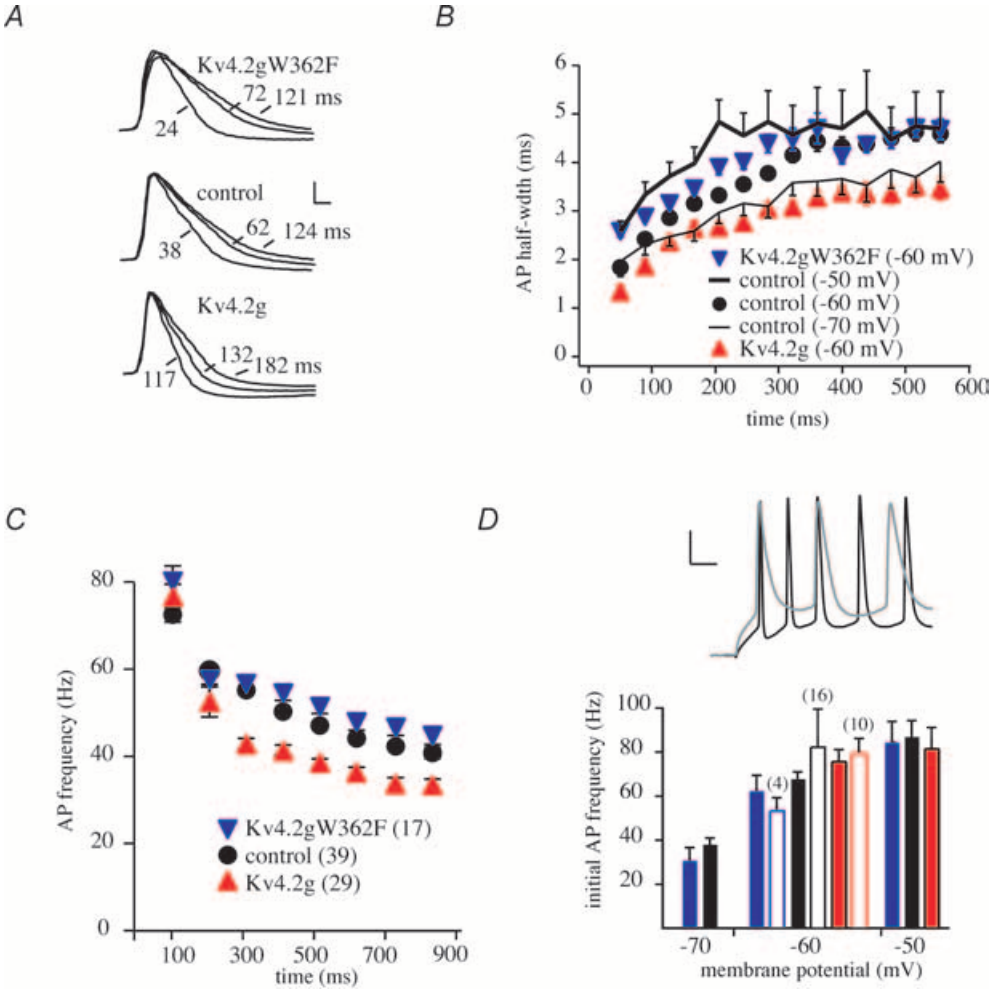

Figure 5. Kv4.2 expression level affects AP half-width and firing frequency in CA1 neurones
A, traces are the voltage responses to a 900 ms, 300 pA current injection in Kv4.2g (bottom traces), control (middle traces), and Kv4.2g^{W362F} (top) neurones at the indicated time during the train, aligned to illustrate half-width. Scale bar: 20 mV, 1 ms. *B*, AP half-width (binned, 50 ms) is plotted *versus* time during a 300 pA current injection. Kv4.2g (red triangles) -expressing cells showed decreased half-widths compared with control neurones (circles) while Kv4.2g^{W362F}-expressing neurones (blue triangles) show broader APs. Lines illustrate the voltage dependency of AP half-width. *C*, firing frequency, calculated from the interspike interval (100 ms bins), plotted against time during a 300 pA current injection for each group. Number of cells in parentheses. *D*, firing frequency during the first 100 ms of the current injection. Top traces show 4-AP (grey trace) reduces AP frequency in a Kv4.2g^{W362F} recording. Scale bar: 20 mV, 50 ms. Grouped data below show firing frequency over first 100 ms of a 300 pA current injection increases with depolarization ($P < 0.05$ for control and Kv4.2g^{W362F}, too few APs were recorded at −70 mV in Kv4.2g-expressing neurones for evaluation) but is not significantly changed with 4-AP (3–5 mM, $P > 0.05$).

to three APs (Fig. 6*A* and *B*, $P < 0.05$). Although the principal effect of Kv4.2g expression is to reduce broadening, broadening actually increased compared with controls by the end of 100 Hz trains (Fig. 6*A* and *C*). A possible explanation for this paradoxical result would be if Kv.4.2 overexpression, decreasing AP half-widths and associated Ca^{2+} influx (see Fig. 8), delays the activation of Ca^{2+}-activated K^+ channels that also have an effect on AP broadening in CA1 neurones (Shao *et al.* 1999).

The initial AP half-width in trains elicited in Kv4.2g^{W362F} neurones did not differ from control (Fig. 6*A*, left column, ▽, $n = 11$, $P > 0.05$). Furthermore, in these cells no significant change in broadening was found between the first and second AP (Fig. 6*B*) indicating

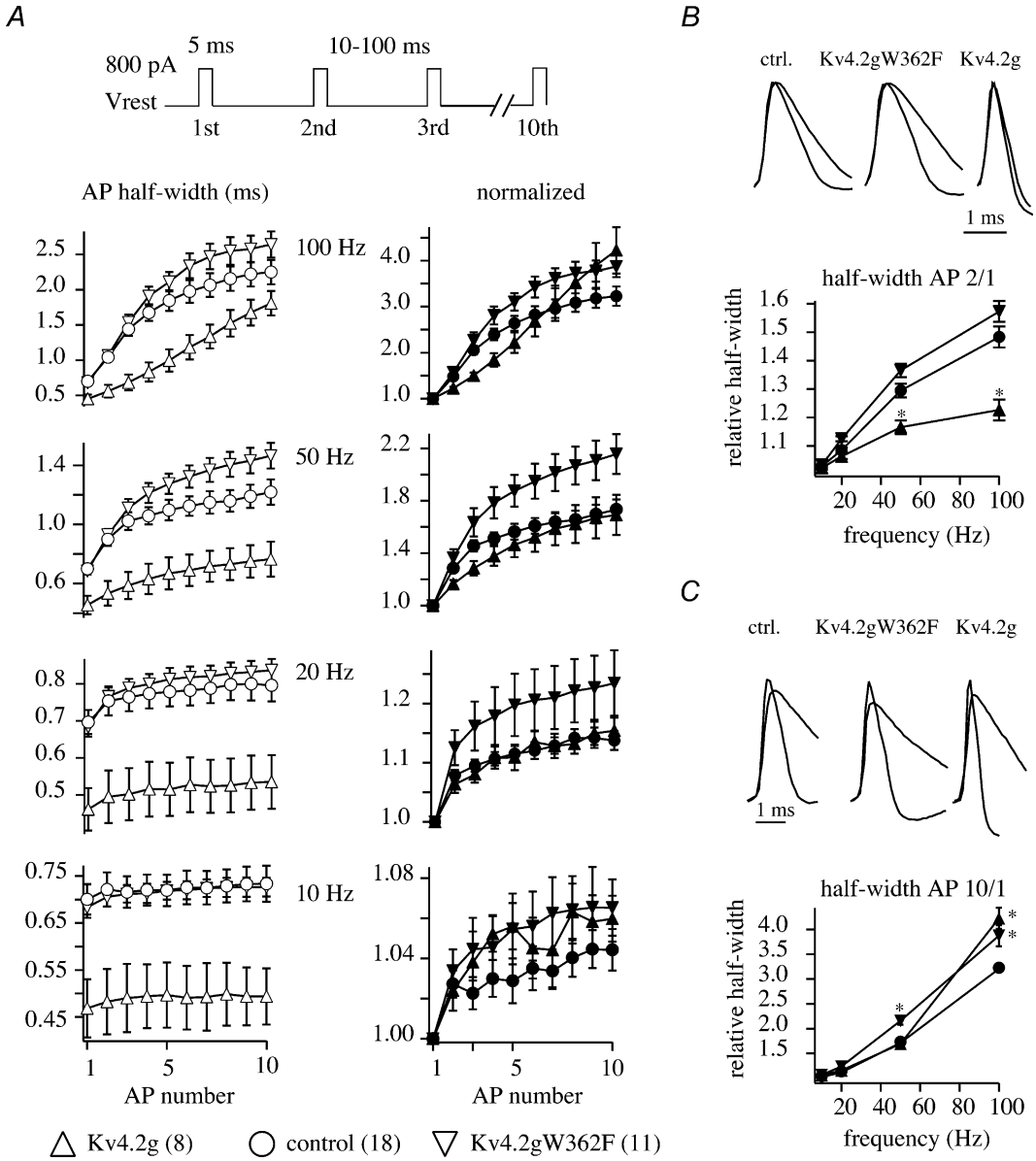

Figure 6. Kv4.2 contributes to frequency-dependent AP broadening in CA1 neurones
A, AP half-widths for each of 10 APs in a train induced at 10, 20, 50 and 100 Hz (left column) are normalized to the first AP of the train (right column) for Kv4.2g- (up triangles), control (circles), and Kv4.2g^{W362F}- (down triangles) expressing neurones. Current protocol is shown above. *B*, Kv4.2g-expressing neurones show significantly reduced broadening between the first and second AP of the train at high frequencies. Traces are the first two action potentials of a 100 Hz train superimposed for each group. *C*, Kv4.2g^{W362F}-overexpressing neurones show increased broadening of the tenth AP at high frequencies. At 100 Hz Kv4.2g also results in a broader AP at the end of the train. Traces are the first and tenth action potentials of a 100 Hz train aligned for each group. $^*P < 0.05$.

residual K^+ conductances (Kv4.2 mediated or other) are sufficient for repolarization of single and pairs of APs. However, cumulative transient channel inactivation occurring during AP trainsleft the half-width larger than control by the end of the high frequency (50 and 100 Hz) trains (Fig. 6*C*, $P < 0.05$). These results support the hypothesis that cumulative Kv4.2 channel inactivation, dependent on fast inactivation and slow recovery from inactivation, contributes to AP broadening in CA1 neurones.

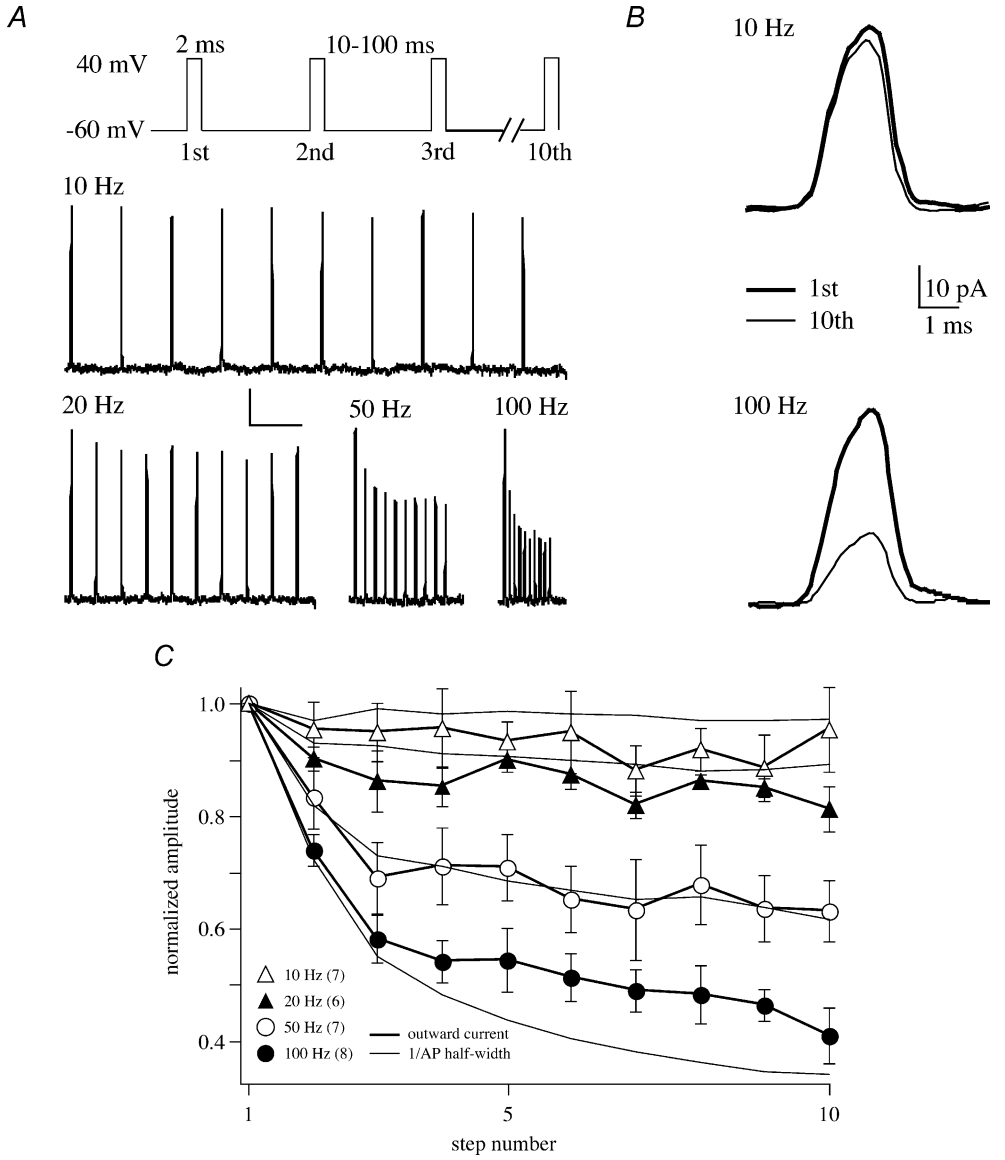

Figure 7. Time course and frequency dependence of native transient current inactivation approximates frequency-dependent AP broadening in CA pyramidal neurones
A, outside-out patch recordings show repetitive activity decreases available transient K^+ currents. To simulate trains of action potentials, trains of 10 depolarizing steps, 2 ms in duration, were delivered to outside-out patches at 10, 20, 50 and 100 Hz. TTX (1 μM) was included in the bath to block Na^+ channels. Leak-subtracted ensemble average of currents show the amplitude of the 10th evoked current is significantly smaller than the amplitude of the first evoked current at 50 and 100 Hz. Scale bar: 10 pA, 100 ms. *B*, first and 10th evoked currents from *A* on expanded time base for 10 and 100 Hz. *C*, group data. To quantify the decrease in current amplitudes during the train, the amplitude of the current evoked by the 10th depolarizing step is plotted as a fraction of the amplitude of the current evoked by the first depolarizing step for each test frequency. Numbers in parentheses indicate the numbers of patches. For comparison, the thin lines represent 1/AP half-width for control neurones at each test frequency (Fig. 6). As expected, given their similar time course of recovery from inactivation (Table 1), Kv4.2g- and Kv4.2g^{W362F}-expressing neurones displayed frequency and time-dependent inactivation not different from control, uninfected neurones (not shown).

If cumulative Kv4.2 channel inactivation does contribute to frequency-dependent AP broadening, the two phenomena should share similar frequency dependencies and time courses. As a test, we measured the frequency response of pharmacologically isolated transient K^+ currents in outside-out patches pulled from somatic membrane neurones of each experimental group. We simulated trains of action potentials in the outside-out patches by trains (10, 20, 50 and 100 Hz) of brief depolarizations (2 ms, −60 to +40 mV steps, Fig. 7*A*). The change in the amplitudes of the ensemble currents was quantified as the relative amplitude of the current evoked by the 10th step in the train compared with the amplitude of the ensemble current evoked by the first (Fig. 7*C*). Figure 7*A* shows typical responses from control neurones for each frequency. At 10 Hz, little inactivation occurs during the train (95 ± 7% remaining). However, at 100 Hz only 40 ± 5% of the transient current remains by the end of the train ($n = 7$; Fig. 7*B* and *C*). Figure 7*C* shows group data for the normalized peak amplitude of the transient current for each test frequency. A comparison to 1/AP half-width (thin lines) reveals that the two cellular processes (cumulative transient K^+ channel inactivation and AP broadening) exhibit similar frequency and activity dependencies. Transient currents from Kv4.2g- and Kv4.2g^{W362F}-expressing neurones displayed similar frequency and activity dependencies (data not shown).

Kv4.2 and back-propagation

Action potentials in CA1 neurones, initiated in the axon, not only propagate down the axon but also back-propagate into dendrites (Jaffe *et al.* 1992; Spruston *et al.* 1995; Stuart

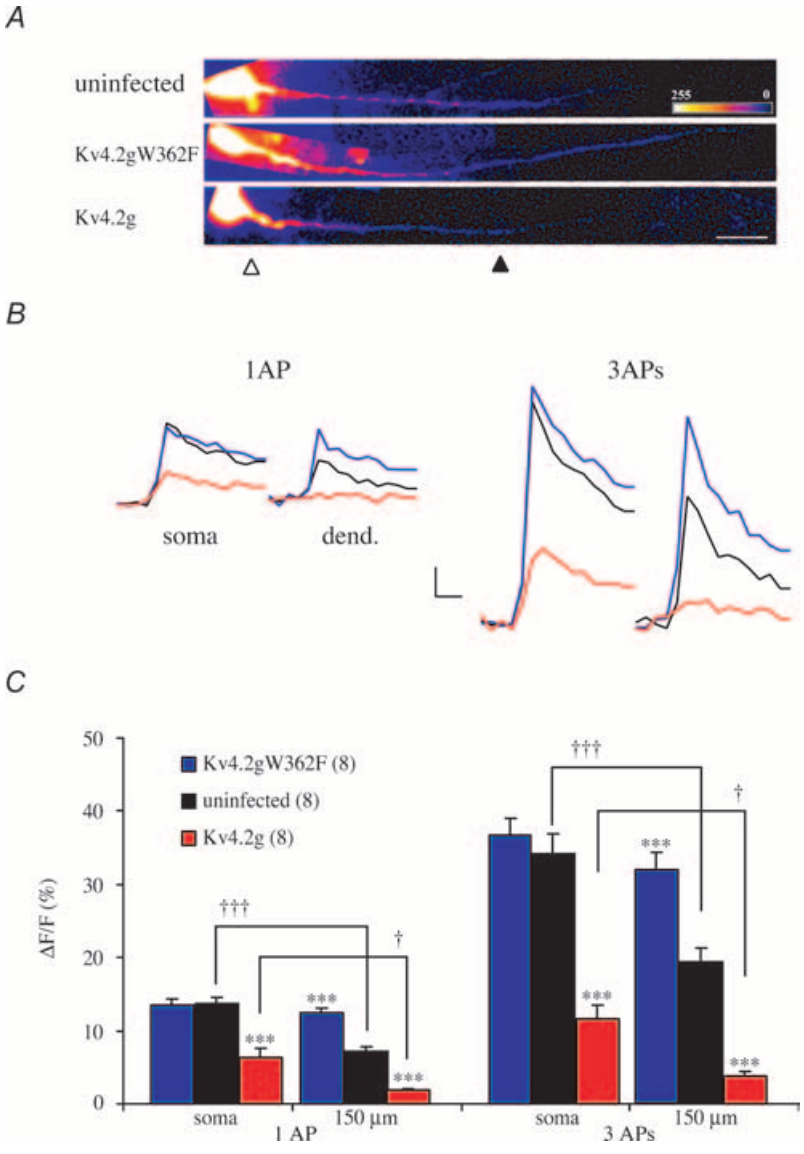

Figure 8. Kv4.2 expression level determines dendritic AP-dependent Ca^{2+} transient amplitudes
A, pseudocolour image illustrating Ca^{2+} influx after three APs (100 Hz) for each experimental group. Triangles indicate somatic (open) and dendritic (150 μm, filled triangle) recording locations. Scale bar, 30 μm; colour scale values are arbitrary units. *B*, representative Ca^{2+} transients evoked by a single and trains of APs recorded from somas (left) and dendrites (150 μm, right) from uninfected (black trace), Kv4.2g- (red trace) and Kv4.2g^{W362F}- (blue trace) expressing neurones. Scale bar, 2.5% $\Delta F/F$, 5 ms. *C*, average peak Ca^{2+} transient for an AP recorded from somas and dendrites (150 μm). Numbers in parentheses are the *n* numbers. ***$P < 0.01$ peak Ca^{2+} difference between experimental group and uninfected neurones; †††$P < 0.01$ peak Ca^{2+} difference between soma and dendrites; †$P < 0.05$ peak Ca^{2+} difference between soma and dendrites. Attenuation of peak Ca^{2+} from soma to dendrite is not significant in Kv4.2g^{W362F} neurones.

et al. 1997; Colbert & Pan, 2002). A high density of transient K^+ currents in CA1 dendrites limits back-propagation, decreasing AP amplitude and associated Ca^{2+} influx (Hoffman *et al.* 1997). We imaged Ca^{2+} influx during single and trains of APs back-propagating in CA1 somas and apical dendrites to test the hypothesis that Kv4-containing channels underlie the transient outward current in CA1 dendrites.

APs evoked by somatic current injection caused Ca^{2+} influx in the soma and apical dendrites in all three experimental groups (Fig. 8*A*). However, compared with uninfected controls, AP-associated Ca^{2+} influx was significantly reduced in both Kv4.2g-expressing somas ($6.4 \pm 1.1\%$, $n = 8$ *versus* $13.8 \pm 0.8\%$, $n = 8$ for control; $P < 0.01$; Fig. 8*B* and *C*) and dendrites ($1.9 \pm 0.2\%$ *versus* $7.2 \pm 2.7\%$ for control; $P < 0.01$; Fig. 8*B* and *C*). A decrease in AP half-width via the increased Kv4.2 density likely accounts for the reduced Ca^{2+} influx in Kv4.2g somata (Fig. 5). Both Kv4.2g and control neurones showed a significant drop in Ca^{2+} influx between the soma and dendrites.

The results from $Kv4.2g^{W362F}$ neurones demonstrate an effect of dendritic Kv4.2 activity on back-propagation. Here, somatic Ca^{2+} transients were no different from control ($13.5 \pm 0.8\%$, $n = 8$, $Kv4.2g^{W362F}$; $13.8 \pm 0.8\%$, $n = 8$, control, Fig. 8*B* and *C*). In the dendrite, however, $Kv4.2g^{W362F}$ neurones exhibited much larger transients ($12.4 \pm 0.8\%$, $n = 8$) than control neurones ($7.2 \pm 2.7\%$, $n = 8$, $P < 0.01$, Fig. 8*B* and *C*) indicating enhanced propagation due to the decrease in functional dendritic Kv4.2 density.

Discussion

Caution is warranted in interpreting the physiological effect of overexpressing voltage-gated channels in neurones. However, the combined use of transient overexpression along with dominant negative mutations provides a more solid and specific interpretation than the typical pharmacological study. Our results show that Kv4 channels (most probably Kv4.2) impact on CA1 excitability over a large voltage range, affecting a number of cellular properties. Expressing the dominant negative mutant, $Kv4.2g^{W362F}$, led to an increased input resistance, broader APs, an increase in frequency-dependent AP broadening during an AP train and enhanced back-propagation. Conversely, Kv4.2 overexpression reduced input resistance, increased AP threshold, delayed AP onset, produced narrower APs with larger initial AHPs, reduced frequency-dependent AP broadening and inhibited dendritic AP propagation. These results, showing that Kv4.2 acts not only as a traditional subthreshold transient current but that it is also active suprathreshold, shaping action potentials and regulating dendritic propagation, represent potential consequences of physiologically altering Kv4.2 activity levels through phosphorylation or auxiliary subunit expression (Hoffman & Johnston, 1998; An *et al.* 2000; Anderson *et al.* 2000; Beck *et al.* 2002; Yuan *et al.* 2002; Nadal *et al.* 2003; Gebauer *et al.* 2004; Varga *et al.* 2004).

Although tending towards the opposite direction of the measured effects in Kv4.2g neurones, no significant effect on first spike latency, AHP, AP threshold or late firing frequency was found for neurones expressing the dominant negative mutation. These negative findings indicate either that the remaining ~60% of Kv4.2 constitutes a sufficient functional density to accomplish these responsibilities or that other non-inactivating types of K^+ channels (e.g. BK or delayed rectifier) are more strongly activated during the current injection than they normally would be in compensation for the reduced functional transient channel activity in these cells.

Kv4 subunits underlie the somatodendritic A-type current in CA1 pyramidal neurones

The data presented here provide direct evidence supporting the hypothesis, previously based on molecular localization studies, that Kv4.2-containing channels are the main contributor to the A-type current recorded in CA1 pyramidal neurones. Outside-out and nucleated patches from $Kv4.2g^{W362F}$-expressing neurones showed a reduced transient current compared with controls. This reduction of current amplitude occurred without an effect on the voltage dependence of steady-state activation or inactivation and current kinetics were equivalent to those recorded in patches from control neurones. Together with immunostaining and *in situ* data suggesting relatively little Kv4.1 and Kv4.3 expression in CA1 pyramidal neurones (Serodio & Rudy, 1998; Rhodes *et al.* 2004) these data strongly implicate Kv4.2 as the main source of the somatodendritic A-current in CA1 neurones.

Subthreshold functions

The activation and inactivation curves of Kv4.2 (Fig. 2*D*) indicate the presence of a significant window current active around the resting membrane potential of CA1 neurones recorded in this study (~ −57 mV). Kv4.2 overexpression increases the strength of this persistent current, reducing the voltage deflection resulting from hyperpolarizing current injection. Decreasing native Kv4 channel activity with $Kv4.2g^{W362F}$ reduces the window current, increasing the voltage response to current injections. A Kv4.2 window current may then act as a shunt to synaptic voltage transients. Modulation of the expression level or steady-state activation or inactivation curve of Kv4.2 (Hoffman & Johnston, 1998; An *et al.* 2000; Yuan *et al.* 2002; Nadal *et al.* 2003; Frick *et al.* 2004; Varga *et al.* 2004)

would then vary the impact of the window current on subthreshold integration. Kv4.2 expression in dendritic spines suggests a mechanism whereby synapse-specific Kv4.2 regulation could contribute to dendritic integration. Further study will be necessary to establish the presence and regulation of Kv4.2 in adult hippocampal CA1 dendritic spines.

Suprathreshold functions

Subsequent to AP initiation, Kv4.2 plays a major role in AP repolarization (Figs 5 and 6) and in limiting AP back-propagation into the dendrites (Fig. 8). At lower frequencies, A-channels are able to recover from inactivation in between APs and so successive APs in trains are of similar half-width (Fig. 6). Recovery from inactivation at low frequencies, allows Kv4.2 to play the classic role of A-channels in regulating repetitive firing (Connor & Stevens, 1971). At high frequencies, however, cumulative inactivation of Kv4.2 results in progressively broader action potentials during the train (Figs 5 and 6). Hence, during high-frequency firing the expression level of Kv4.2 will have a large impact on the time course and degree of cellular Ca^{2+} influx and those processes that are Ca^{2+}-dependent second messenger cascades such as gene expression and synaptic plasticity.

References

Aldrich RW Jr, Getting PA & Thompson SH (1979). Mechanism of frequency-dependent broadening of molluscan neurone soma spikes. *J Physiol* **291**, 531–544.

Alonso G & Widmer H (1997). Clustering of KV4.2 potassium channels in postsynaptic membrane of rat supraoptic neurons: an ultrastructural study. *Neuroscience* **77**, 617–621.

An WF, Bowlby MR, Betty M, Cao J, Ling HP, Mendoza G, Hinson JW, Mattsson KI, Strassle BW, Trimmer JS & Rhodes KJ (2000). Modulation of A-type potassium channels by a family of calcium sensors. *Nature* **403**, 553–556.

Anderson AE, Adams JP, Qian Y, Cook RG, Pfaffinger PJ & Sweatt JD (2000). Kv4.2 phosphorylation by cyclic AMP-dependent protein kinase. *J Biol Chem* **275**, 5337–5346.

Andreasen M & Lambert JD (1995). Regenerative properties of pyramidal cell dendrites in area CA1 of the rat hippocampus. *J Physiol* **483**, 421–441.

Bahring R, Boland LM, Varghese A, Gebauer M & Pongs O (2001). Kinetic analysis of open- and closed-state inactivation transitions in human Kv4.2 A-type potassium channels. *J Physiol* **535**, 65–81.

Baro DJ, Levini RM, Kim MT, Willms AR, Lanning CC, Rodriguez HE & Harris-Warrick RM (1997). Quantitative single-cell-reverse transcription-PCR demonstrates that A-current magnitude varies as a linear function of shal gene expression in identified stomatogastric neurons. *J Neurosci* **17**, 6597–6610.

Barry DM, Xu H, Schuessler RB & Nerbonne JM (1998). Functional knockout of the transient outward current, long-QT syndrome, and cardiac remodeling in mice expressing a dominant-negative Kv4 alpha subunit. *Circ Res* **83**, 560–567.

Beck EJ, Bowlby M, An WF, Rhodes KJ & Covarrubias M (2002). Remodelling inactivation gating of Kv4 channels by KChIP1, a small-molecular-weight calcium-binding protein. *J Physiol* **538**, 691–706.

Cai X, Liang CW, Muralidharan S, Kao JP, Tang CM & Thompson SM (2004). Unique roles of SK and Kv4.2 potassium channels in dendritic integration. *Neuron* **44**, 351–364.

Cash S & Yuste R (1998). Input summation by cultured pyramidal neurons is linear and position-independent. *J Neurosci* **18**, 10–15.

Coetzee WA, Amarillo Y, Chiu J, Chow A, Lau D, McCormack T, Moreno H, Nadal MS, Ozaita A, Pountney D, Saganich M, Vega-Saenz De Miera E & Rudy B (1999). Molecular diversity of K^+ channels. *Ann N Y Acad Sci* **868**, 233–285.

Colbert CM & Pan E (2002). Ion channel properties underlying axonal action potential initiation in pyramidal neurons. *Nat Neurosci* **5**, 533–538.

Connor JA & Stevens CF (1971). Prediction of repetitive firing behaviour from voltage clamp data on an isolated neurone soma. *J Physiol* **213**, 31–53.

Faber ES & Sah P (2003). Ca^{2+}-activated K^+ (BK) channel inactivation contributes to spike broadening during repetitive firing in the rat lateral amygdala. *J Physiol* **552**, 483–497.

Frick A, Magee J & Johnston D (2004). LTP is accompanied by an enhanced local excitability of pyramidal neuron dendrites. *Nat Neurosci* **7**, 126–135.

Gebauer M, Isbrandt D, Sauter K, Callsen B, Nolting A, Pongs O & Bahring R (2004). N-type inactivation features of Kv4.2 channel gating. *Biophys J* **86**, 210–223.

Geiger JR & Jonas P (2000). Dynamic control of presynaptic Ca^{2+} inflow by fast-inactivating K^+ channels in hippocampal mossy fiber boutons. *Neuron* **28**, 927–939.

Hoffman DA & Johnston D (1998). Downregulation of transient K^+ channels in dendrites of hippocampal CA1 pyramidal neurons by activation of PKA and PKC. *J Neurosci* **18**, 3521–3528.

Hoffman DA, Magee JC, Colbert CM & Johnston D (1997). K^+ channel regulation of signal propagation in dendrites of hippocampal pyramidal neurons. *Nature* **387**, 869–875.

Jaffe DB, Johnston D, Lasser-Ross N, Lisman JE, Miyakawa H & Ross WN (1992). The spread of Na^+ spikes determines the pattern of dendritic Ca^{2+} entry into hippocampal neurons. *Nature* **357**, 244–246.

Jerng HH, Pfaffinger PJ & Covarrubias M (2004). Molecular physiology and modulation of somatodendritic A-type potassium channels. *Mol Cell Neurosci* **27**, 343–369.

Johns DC, Nuss HB & Marban E (1997). Suppression of neuronal and cardiac transient outward currents by viral gene transfer of dominant-negative Kv4.2 constructs. *J Biol Chem* **272**, 31598–31603.

Kim J, Dittgen T, Nimmerjahn A, Waters J, Pawlak V, Helmchen F, Schlesinger S, Seeburg PH & Osten P (2004). Sindbis vector SINrep (nsP2S726): a tool for rapid heterologous expression with attenuated cytotoxicity in neurons. *J Neurosci Meth* **133**, 81–90.

Lien CC, Martina M, Schultz JH, Ehmke H & Jonas P (2002). Gating, modulation and subunit composition of voltage-gated K^+ channels in dendritic inhibitory interneurones of rat hippocampus. *J Physiol* **538**, 405–419.

Ma M & Koester J (1996). The role of K^+ currents in frequency-dependent spike broadening in Aplysia R20 neurons: a dynamic-clamp analysis. *J Neurosci* **16**, 4089–4101.

Maletic-Savatic M, Lenn NJ & Trimmer JS (1995). Differential spatiotemporal expression of K^+ channel polypeptides in rat hippocampal neurons developing in situ and in vitro. *J Neurosci* **15**, 3840–3851.

Malin SA & Nerbonne JM (2000). Elimination of the fast transient in superior cervical ganglion neurons with expression of KV4.2W362F: molecular dissection of IA. *J Neurosci* **20**, 5191–5199.

Malin SA & Nerbonne JM (2001). Molecular heterogeneity of the voltage-gated fast transient outward K^+ current, I_{Af}, in mammalian neurons. *J Neurosci* **21**, 8004–8014.

Martina M, Schultz JH, Ehmke H, Monyer H & Jonas P (1998). Functional and molecular differences between voltage-gated K^+ channels of fast-spiking interneurons and pyramidal neurons of rat hippocampus. *J Neurosci* **18**, 8111–8125.

Musleh W, Yaghoubi S & Baudry M (1997). Effects of a nitric oxide synthase inhibitor on NMDA receptor function in organotypic hippocampal cultures. *Brain Res* **770**, 298–301.

Nadal MS, Ozaita A, Amarillo Y, Vega-Saenz De Miera E, Ma Y, Mo W, Goldberg EM, Misumi Y, Ikehara Y, Neubert TA & Rudy B (2003). The CD26-related dipeptidyl aminopeptidase-like protein DPPX is a critical component of neuronal A-type K^+ channels. *Neuron* **37**, 449–461.

Osten P, Srivastava S, Inman GJ, Vilim FS, Khatri L, Lee LM, States BA, Einheber S, Milner TA, Hanson PI & Ziff EB (1998). The AMPA receptor GluR2 C terminus can mediate a reversible, ATP-dependent interaction with NSF and alpha- and beta-SNAPs. *Neuron* **21**, 99–110.

Ramakers GM & Storm JF (2002). A postsynaptic transient K^+ current modulated by arachidonic acid regulates synaptic integration and threshold for LTP induction in hippocampal pyramidal cells. *Proc Natl Acad Sci U S A* **99**, 10144–10149.

Rhodes KJ, Carroll KI, Sung MA, Doliveira LC, Monaghan MM, Burke SL, Strassle BW, Buchwalder L, Menegola M, Cao J, An WF & Trimmer JS (2004). KChIPs and Kv4 alpha subunits as integral components of A-type potassium channels in mammalian brain. *J Neurosci* **24**, 7903–7915.

Rudy B (1988). Diversity and ubiquity of K channels. *Neuroscience* **25**, 729–749.

Serodio P & Rudy B (1998). Differential expression of Kv4 K^+ channel subunits mediating subthreshold transient K^+ (A-type) currents in rat brain. *J Neurophysiol* **79**, 1081–1091.

Serodio P, Vega-Saenz De Miera E & Rudy B (1996). Cloning of a novel component of A-type K^+ channels operating at subthreshold potentials with unique expression in heart and brain. *J Neurophysiol* **75**, 2174–2179.

Shao LR, Halvorsrud R, Borg-Graham L & Storm JF (1999). The role of BK-type Ca^{2+}-dependent K^+ channels in spike broadening during repetitive firing in rat hippocampal pyramidal cells. *J Physiol* **521**, 135–146.

Sheng M, Tsaur ML, Jan YN & Jan LY (1992). Subcellular segregation of two A-type K^+ channel proteins in rat central neurons. *Neuron* **9**, 271–284.

Shibata R, Misonou H, Campomanes CR, Anderson AE, Schrader LA, Doliveira LC, Carroll KI, Sweatt JD, Rhodes KJ & Trimmer JS (2003). A fundamental role for KChIPs in determining the molecular properties and trafficking of Kv4.2 potassium channels. *J Biol Chem* **278**, 36445–36454.

Shibata R, Nakahira K, Shibasaki K, Wakazono Y, Imoto K & Ikenaka K (2000). A-type K^+ current mediated by the Kv4 channel regulates the generation of action potential in developing cerebellar granule cells. *J Neurosci* **20**, 4145–4155.

Song WJ, Tkatch T, Baranauskas G, Ichinohe N, Kitai ST & Surmeier DJ (1998). Somatodendritic depolarization-activated potassium currents in rat neostriatal cholinergic interneurons are predominantly of the A type and attributable to coexpression of Kv4.2 and Kv4.1 subunits. *J Neurosci* **18**, 3124–3137.

Spruston N, Schiller Y, Stuart G & Sakmann B (1995). Activity-dependent action potential invasion and calcium influx into hippocampal CA1 dendrites. *Science* **268**, 297–300.

Storm JF (1990). Potassium currents in hippocampal pyramidal cells. *Prog Brain Res* **83**, 161–187.

Stuart G, Spruston N, Sakmann B & Hausser M (1997). Action potential initiation and backpropagation in neurons of the mammalian CNS. *Trends Neurosci* **20**, 125–131.

Tkatch T, Baranauskas G & Surmeier DJ (2000). Kv4.2 mRNA abundance and A-type K^+ current amplitude are linearly related in basal ganglia and basal forebrain neurons. *J Neurosci* **20**, 579–588.

Varga AW, Anderson AE, Adams JP, Vogel H & Sweatt JD (2000). Input-specific immunolocalization of differentially phosphorylated Kv4.2 in the mouse brain. *Learn Mem* **7**, 321–332.

Varga AW, Yuan LL, Anderson AE, Schrader LA, Wu GY, Gatchel JR, Johnston D & Sweatt JD (2004). Calcium-calmodulin-dependent kinase II modulates Kv4.2 channel expression and upregulates neuronal A-type potassium currents. *J Neurosci* **24**, 3643–3654.

Watanabe S, Hoffman DA, Migliore M & Johnston D (2002). Dendritic K^+ channels contribute to spike-timing dependent long-term potentiation in hippocampal pyramidal neurons. *Proc Natl Acad Sci U S A* **99**, 8366–8371.

Wong W, Newell EW, Jugloff DGM, Jones OT & Schlichter LC (2002). Cell surface targeting and clustering interactions between heterologously expressed PSD-95 and the Shal voltage-gated potassium channel, Kv4.2. *J Biol Chem* **277**, 20423–20430.

Yuan LL, Adams JP, Swank M, Sweatt JD & Johnston D (2002). Protein kinase modulation of dendritic K^+ channels in hippocampus involves a mitogen-activated protein kinase pathway. *J Neurosci* **22**, 4860–4868.

Acknowledgements

This work was supported by the Intramural Research Program of the National Institutes of Health and the National Institute of Child Health and Human Development. We thank Arrash Yazdani for tissue culture and transfections, and Josh Lawrence and Andres Buonanno for their critical review of the manuscript. The potassium channel antibody (K57/1) was a gift from Dr James Trimmer (University of California, Davis, School of Medicine).

Supplemental material

The online version of this paper can be accessed at:
DOI: 10.1113/jphysiol.2005.095042
http://jp.physoc.org/cgi/content/full/jphysiol.2005.095042/DC1
and contains supplemental material including one figure entitled: Kv4.2 constructs.

This material can also be found as part of the full-text HTML version available from http://www.blackwell-synergy.com